 CMES, vol.112, no.1, pp.59-73, 2016

Applying a Step Approach Method in Solving the Multi-Frequency Radiation From a Complex Obstacle

Jui-Hsiang Kao[1]

Abstract: In this paper, a step approach method in the time domain is developed to calculate the radiated waves from an arbitrary obstacle pulsating with multiple frequencies. The computing scheme is based on the Boundary Integral Equation and derived in the time domain; thus, the time-harmonic Neumann boundary condition can be imposed. By the present method, the values of the initial conditions are set to zero, and the approach process is carried forward in a loop from the first time step to the last. At each time step, the radiated pressure on each element is updated. After several loops, the correct radiated pressures can be obtained.
A sphere pulsating with a monopole frequency in an infinite acoustic domain is calculated first. This result is compared with the analytical solution, and both of them are in good agreement. Then, a complex-shaped radiator is taken as the studied case. The pulsating frequency of this case is multiple, and the waves propagate in half space. It is shown that the present method can treat multiple-frequency pulsation well, even when the radiator is a complex shape, and a robust convergence can be attained quickly.

Keywords: Step approach method; Time domain; Radiated waves; Multiple frequencies; Boundary integral equation; Neumann boundary condition.

1 Introduction

The radiated waves from any pulsating obstacle in air or underwater are detected for many reasons, such as remote sensing and military defense. In general, the obstacle is often arbitrarily shaped, and the pulsation of a multi-frequency.

Early works have solved the radiation from a pulsating obstacle in the frequency domain. Since the1960s, researchers such as Schenck (1968); Burton and Miller (1971) have attempted to resolve radiating problems based on an integral equation

[1] Department of Systems Engineering and Naval Architecture, National Taiwan Ocean University, Keelung, Taiwan, R.O.C.

in the exterior domain. Schenck (1968) introduced the CHIEF method to overcome the problem of non-unique solutions at fictitious eigenfrequencies. Seybert, Soenarko, Rizzo, and Shippy (1985) developed a second-order boundary element method in the frequency domain, and [Seybert and Soenarko (1988)] derived the formulations in the infinite half-space. Seybert and Wu (1988); Li, Wu, and Seybert (1994) discussed arbitrary impedance on an infinite free surface. Chaosong (1993) derived a direct boundary integral equation method in the frequency domain. Kress and Mohsen (1986); Ochmann (1995) developed the source simulation technique (SST) in the frequency domain for faster computation of complex structures. Wu (1994) solved the radiation in a perfect waveguide. Wu (1995) applied the direct boundary element method in computing the radiation from a regular and thin body. In Qian, Han, Ufimtsev, and Atluri (2004), the non-hyper-singular boundary integral equation was derived to solve the non-uniqueness problem involved in the composite Helmholtz integral equation. Normal vector of elemental node was defined and applied to avoid the indefinite normal vector and the discontinuous normal velocity at sharp edges and corners by Zai (2006). Qian, Han, and Atluri (2013) proposed the fast multipole method, FMM-BEM, to overcome the drawback of fully populated system matrices in BEM.

The time-domain method is a better choice for an obstacle pulsating with a multi-frequency. Mansur and Brebbia (1982); Groenbroom (1983); Dohner, Shoureshi, and Bernhard (1987); Araújo, Mansur, and Carrer (2000) derived time-domain boundary element formulations for transient problems. According to Araújo, Mansur, and Carrer (2000), numerical errors propagate forward in time and result in incorrect solutions. In Kropp and Svensson (1995), the time-domain formulations of equivalent sources were used to approximate the Green's functions of small volume sources in front of arbitrarily shaped structures to simplify the radiation problem. Jang and Ih (2012) filtered the troublesome wave vectors at each time step in the time-domain boundary method to stabilize the time step marching. Bi, Lin, and Zhang (2013) solved the transient acoustic radiation from an arbitrarily shaped source in the time domain using a cubic spline interpolation. In Mikael and Masami (2013), a simple axi-symmetric model was solved by the time-domain boundary element method. In Zheng, Bi, Zhang, and Xu (2015), the time-domain equivalent source method (TESM) was used to calculate the radiated waves. The TESM results showed an instability due to the errors amplified exponentially with time; thus, time averaging was applied in the iterative process to reduce the instability.

In this paper, a step approach method in the time domain is derived to solve the radiation from an obstacle pulsating with multiple frequencies. The Green's function in the boundary integral equation is combined in forms relative to the retarded time;

thus, the marching process becomes easier. The radiated pressure on each element can be expressed by a source term and a dipole term. The time-harmonic Neumann boundary condition is applied in the source term and known. The initial values of the radiated pressures in the dipole term are set as zero. The time interpolation is replaced by a Fourier series to minimize numerical error due to time interpolation. The stability and reliability of the present method will be evidenced.

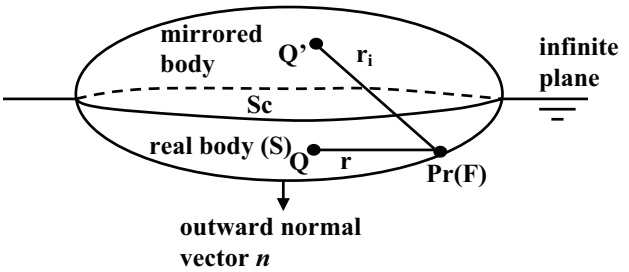

Figure 1: A body of arbitrary shape on a semi-infinite plane.

2 Theoretical formulations

An arbitrarily shaped body immersed in a semi-infinite domain is considered, as shown in Figure 1. The body surface is denoted by S, its outward normal by n, the radiated acoustic pressure by P_r and the interface of the body and the infinite plane by Sc. The infinite plane of the interface can be simulated by a mirror-image body. By applying Green's second identity and the Sommerfeld radiation condition, a boundary integral equation is defined on S:

$$C(F)P_r(F) = \int_S \left(P_r(Q)\frac{\partial G(F,Q)}{\partial n} - G(F,Q)\frac{\partial P_r(Q)}{\partial n} \right) \mathrm{d}S. \tag{1}$$

$G(F,Q)$ is the half-space Green's function that depends on both locations of a field point, F, and a source point, Q:

$$G(F,Q) = \frac{1}{4\pi}\left(\frac{e^{-ikr}}{r} + R_H \frac{e^{-ikr_i}}{r_i} \right), \tag{2}$$

where r is the distance between F and Q, and r_i is the distance between P and Q', the imaged point of Q, as shown in Figure 1. The reflection coefficient, R_H, is equal to 1 for a rigid infinite plane, and -1 for a soft infinite plane. $C(F)$ in Equation (1) is the solid angle for the field point, F, and can be evaluated as follows (see e.g.,

Seybert and Wu (1988)):

$$C(F) = 1 + \frac{1}{4\pi}\int_{S+S_c} \frac{\partial}{\partial n}\left[\frac{1}{r(F,Q)}\right] \mathrm{d}S \tag{3}$$

if F is on S, but not in contact with S_c, and

$$C(F) = (1+R_H)\left\{\frac{1}{2} + \frac{1}{4\pi}\int_{S+S_c} \frac{\partial}{\partial n}\left[\frac{1}{r(F,Q)}\right] \mathrm{d}S\right\} \tag{4}$$

if F is on the intersection of S and S_c.

Equation (1) can be expressed in the time domain by the inverse Fourier transform.

$$\begin{aligned} & C(F)P_r(F,t) \\ &= \int_{-\infty}^{\infty}\int_S P_r(Q)\cdot\frac{\partial G(F,Q)}{\partial n}\cdot \mathrm{e}^{\mathrm{i}\omega t}\mathrm{d}S\mathrm{d}\omega - \int_{-\infty}^{\infty}\int_S G(F,Q)\cdot\frac{\partial P_r(Q)}{\partial n}\cdot \mathrm{e}^{\mathrm{i}\omega t}\mathrm{d}S\mathrm{d}\omega. \\ &= \text{Dipole Term} + \text{Source Term} \end{aligned} \tag{5}$$

Because the first term on the right-hand side of Equation (5) is relative to the unit dipole strength, $\dfrac{\partial(1/r)}{\partial n}$, it is named the Dipole Term. Similarly, the second term on the right-hand side of Equation (5) is associated with the unit source strength, $1/r$; therefore, it is named the Source Term.

3 Step approach method

The half-space Green's function in Equation (2) can be combined with the exponent term, e^{iwt}, in Equation (5). Thus, the delay time of wave propagation, t-r/c, can be presented in the dipole term and the source term. Take the dipole term in Equation (5) for example, which can be rewritten as follows:

$$\begin{aligned} \text{Dipole Term} = & \frac{1}{4\pi}\int_{-\infty}^{\infty}\int_S P_r(Q)\cdot\frac{\partial\left(e^{-ikr}/r\right)}{\partial n}\cdot \mathrm{e}^{\mathrm{i}\omega t}\mathrm{d}S\mathrm{d}\omega \\ & + R_H\frac{1}{4\pi}\int_{-\infty}^{\infty}\int_S P_r(Q)\cdot\frac{\partial\left(e^{-ikr_i}/r_i\right)}{\partial n_{\mathrm{i}}}\cdot \mathrm{e}^{\mathrm{i}\omega t}\mathrm{d}S\mathrm{d}\omega \end{aligned} \tag{6}$$

The first term on the right-hand side of Equation (6) is rearranged as follows:

$$\frac{1}{4\pi}\int_{-\infty}^{\infty}\int_S P_r(Q)\cdot\frac{\partial\left(e^{-ikr}/r\right)}{\partial n}\cdot \mathrm{e}^{\mathrm{i}\omega t}\mathrm{d}S\mathrm{d}\omega = \tag{7}$$

$$\frac{1}{4\pi}\int_S \left[P_r(Q,t-r/c)\cdot\frac{\partial(1/r)}{\partial n}\right]\mathrm{d}S+\frac{1}{4\pi}\int_S \left[\frac{\partial P_r(Q,t-r/c)}{\partial t}\cdot\frac{r}{c}\cdot\frac{\partial(1/r)}{\partial n}\right]\mathrm{d}S.$$

Thus, the dipole term can be expressed in the time domain as below:

$$\text{Dipole Term}=\sum_{m=1}^{M}\left\{\begin{array}{l}\left[P_r(Q,t-r/c)\cdot\left(\frac{-1}{r^2}\right)-\frac{\partial P_r(Q,t-r/c)}{\partial t}\cdot\frac{1}{cr}\right]\\ \quad\cdot(\nabla\vec{r}.\vec{n})+R_H\cdot\left[P_r(Q,t-r_i/c)\cdot\left(\frac{-1}{r_i^2}\right)\right.\\ \quad\left.-\frac{\partial P_r(Q,t-r_i/c)}{\partial t}\cdot\frac{1}{cr_i}\right]\cdot(\nabla\vec{r}_i.\vec{n}_i)\end{array}\right\}_m\cdot\frac{\Delta S_m}{4\pi}. \tag{8}$$

It is noted that during the computing process, all the retarded-time terms in Equation (8) can be obtained directly from the Fourier series:

$$P_r(Q,t-r/c)=A_0(Q)+\sum_{n=1}^{\infty}A_n(Q)\cdot\cos[n\omega(t-r/c)]+B_n(Q)\cdot\sin[n\omega(t-r/c)] \tag{9}$$

$$\frac{\partial P_r(Q,t-r/c)}{\partial t}=n\omega\left\{\sum_{n=1}^{\infty}-A_n(Q)\cdot\sin[n\omega(t-r/c)]+B_n(Q)\cdot\cos[n\omega(t-r/c)]\right\} \tag{10}$$

Because the time interpolations of $P_r(Q,t-r/c)$ and $\partial P_r(Q,t-r/c)/\partial t$ in the time domain are expressed in close forms, the numerical errors generated by the time interpolations are minimized.

By applying the Neumann boundary condition and presenting the normal velocity by the time-harmonic form, the source term in Equation (5) can be expressed as:

$$\begin{aligned}\text{Source Term}&=-\int_{-\infty}^{\infty}\int_S G(F,Q)\cdot\frac{\partial P_r(Q)}{\partial n}\cdot\mathrm{e}^{\mathrm{i}\omega\mathrm{t}}\mathrm{d}S\mathrm{d}\omega\\&=\frac{-1}{4\pi}\int_S\left[\left(\frac{1}{r}\right)\cdot\frac{\partial P_r(Q,t-r/c)}{\partial n}\right]\mathrm{d}S\\&\quad-\frac{R_H}{4\pi}\int_S\left[\left(\frac{1}{r_i}\right)\cdot\frac{\partial P_r(Q,t-r_i/c)}{\partial n_i}\right]\mathrm{d}S\\&=\sum_{m=1}^{M}\left\{\left[\sum_{J=1}^{\infty}i\omega_j\rho V_j(Q)\,e^{i\omega_j\left(t-\frac{r}{c}\right)}\right]\cdot\frac{1}{r}\right.\end{aligned}$$

$$+R_H \cdot \left[\sum_{J=1}^{\infty} i\omega_j \rho V_j(Q) e^{i\omega_j \left(t-\frac{r_j}{c}\right)} \right] \cdot \frac{1}{r_i} \Bigg\}_m \cdot \frac{\Delta S_m}{4\pi}. \tag{11}$$

where ρ is the mean density of the fluid, V_j is the amplitude of the normal velocity and ω_j the angular frequency of V_j. In Equations (8) and (11), the oscillatory integrals in the boundary integral equation are expressed in forms relative to the retarded time, which makes the iteration process easier.

The step approach method is based on Equation (5). The source term in Equation (11) is a boundary condition and known. An initial radiated pressure, P_r, on the body equal to zero is first prescribed. Then, the radiated pressure field on the body on the left-hand side of Equation (5) can be updated explicitly by calculating the dipole term according to Equations (8) $\sim$ (10).

The time step is repeated over the longest period ($T = 1/f_{MIN}$) of the multi-frequency pulsation of the obstacle. This approach process is repeated until the proper convergence is achieved. The time marching is divided into n time steps (ISTEP $=$ n) within the longest period.

The procedure of the present scheme is indicated by an example shown in Figure 2. In Figure 2, there is a total of three elements ($1 \sim 3$) on the obstacle, and the time marching is divided into 3 time steps within the longest period. For the first loop, the initial radiated pressure of every element at each time step is set as zero. At the first time step, the radiated pressure of every element is updated according to the right-hand side of Equation (5). The updated values are P_{111}, P_{211} and P_{311}. Similarly, the updated values of each element at the 3rd time step are P_{131}, P_{231} and P_{331} individually. As the first loop is finished, the radiated pressures on all elements are updated. Then, the updated values of the first loop are used as the initial values for the second loop, and the approach process is the same as that of the first loop. After several loops, a robust convergence can be achieved, and the corrected radiated pressure on each element is approached within an acceptable numerical error.

4 Numerical results

The radiated pressure by a sphere pulsating with a mono-frequency in an infinite domain is calculated first. This result is compared with the analytical solution in order to verify the present method. Then, an arbitrarily complex obstacle in the half-space domain is studied. The pulsating frequency of the complex obstacle is multi-frequency. The geometry of the complex obstacle includes sharp edges, an apex and an enormous variation in curvature.

Figure 2: Flow chart of the numerical implementation.

4.1 Sphere pulsating with mono-frequency

Figure 3 shows a pulsating sphere of radius (R) 1 m in an infinite air domain. The mean density of the air is 1.21 kg/m^3, and the sound speed is 343 m/s. The pulsating frequency of $f = 54.59$ (i.e., $KR = 1$) is selected. The normal velocity amplitude, V_n, is assumed to be one. A total of 1800 elements are used to model the sphere.

The present scheme is used to plot the convergence history, as shown in Figure 4, which is easily done. The maximum difference of radiated pressure on any element between the $(n+1)$th and nth loops ($P_{r,n+1} - P_{r,n}$) is less than 10^{-4} (Pa) after the eighth loop, and the convergent value of the radiated pressure is 292.3 Pa.

The analytical solution for this case is:

$$P_r = \left(\frac{R^2}{r}\right) \frac{i\rho\omega}{1+ikR} e^{-ik(r-R)}. \tag{12}$$

According to Equation (12), the analytical solution for this case is 293.4 Pa. The error between the numerical and analytical solutions is about 0.37%. From this case, it is shown that the numerical solution compares well with the analytical one, and that the present method is both stable and reliable.

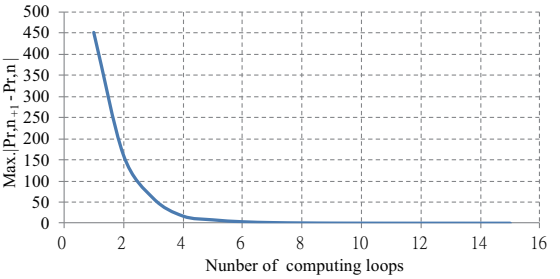

Figure 3: Sphere in the infinite air domain for the case in 4.1.

Figure 4: Convergence history for the case in 4.1.

4.2 Arbitrarily complex obstacle pulsating with multiple frequencies

In Figure 5, an arbitrary obstacle composed by a cube (Faces $1 \sim 4$) and a pyramid (Face 5) in the half-space domain is treated as the studied case. The complex geometry includes sharp edges, an apex and an enormous variation in curvature. The side length of the cube is 1 m, and the center is at (0, 0, 0). The X-Y plane is thought of as an infinite plane. The infinite plane is considered to be rigid, and simulated by a positive image, i.e., RH $= 1$. The mean density of the air is 1.21 kg/m^3, and the sound speed is 343 m/s.

The pulsating frequencies and amplitudes of this obstacle are listed in Table 1.

The time step over the longest period is 20 (i.e., $\Delta t = 0.0025$ s) and the number of elements on the obstacle is 980. The maximum side length of the elements to the minima wave length, $l_{\max}/\lambda$, is 0.0208.

The convergence history, as shown in Figure 6, indicates the present procedure

Figure 5: A complex radiator in the half-space domain for the case in 4.2.

Figure 6: Convergence history for the case in 4.2.

Table 1: Pulsating frequencies and amplitudes for the case in 4.2.

Normal velocity amplitude (V_j, $j = 1 \sim 5$)	Corresponding angular frequency (ω_j, $j = 1 \sim 5$)
$V_1 = 1$	$\omega_1 = 2\pi \times 20$
$V_2 = 1$	$\omega_2 = 2\pi \times 40$
$V_3 = 1$	$\omega_3 = 2\pi \times 60$
$V_4 = 1$	$\omega_4 = 2\pi \times 80$
$V_5 = 1$	$\omega_5 = 2\pi \times 100$

to be robustly convergent, with only 13 loops needed to reached an error under 10^{-4} (Pa). Because the pulsating frequencies of the obstacle are from f to $5f$, the amplitudes and phase angles of the radiated pressure, $D(F)_q$ and $\theta(F)_q$, vanish for $q \neq 1 \sim 5$. The amplitudes of the first harmonic, $D(F)_1$ (Pa), computed by the present method on Faces 1 and 2, are almost the same, as shown in Figure 7. As the elements are closer to the infinite plane, the radiated amplitudes are stronger due to the positive image. The values on Face 5, as plotted in Figure 8, show the contours to be symmetrical with respect to the central point, because the obstacle is symmetrical with respect to that point.

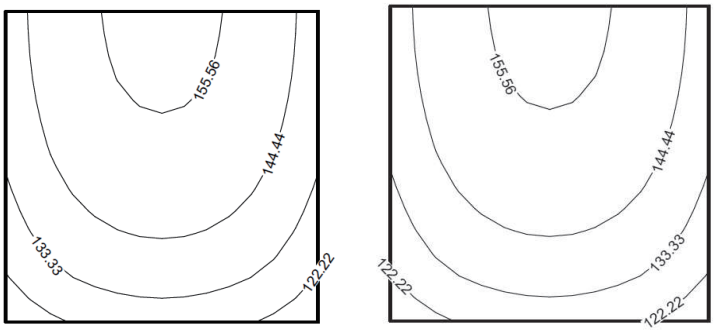

Figure 7: $D(F)_1$ (Pa) on Faces 1 and 2 for the case in 4.2.

The amplitudes of the fifth harmonic, $D(F)_5$ (Pa), computed by the present method on Faces 1, 2 and 5 are shown in Figures 9 and 10, respectively. The distributions are similar to those shown in Figures 7 and 8. However, the values of $D(F)_5$ are larger than those of $D(F)_1$ because the source term in Equation (11) is a function of the angular frequency, ω.

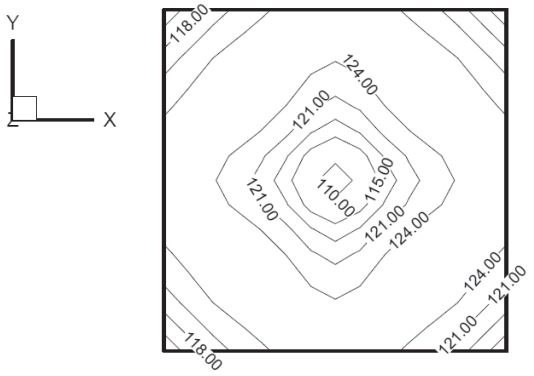

Figure 8: $D(F)_1$ (Pa) on Face 5 for the case in 4.2.

4.3 Stability test

The stability of the present method is tested using the same obstacle as shown in Figure 5, and the pulsating conditions listed in Table 1 are applied.

The ratio of the maximum side length of the elements to the minima wave length, $l_{\max}/\lambda$, is kept as 0.0208; however, the number of time steps over the longest period is changed. The convergence histories with different time steps, as plotted in Figure 11, reveal that more than 10 time steps are required for the present method to prevent numerical divergence.

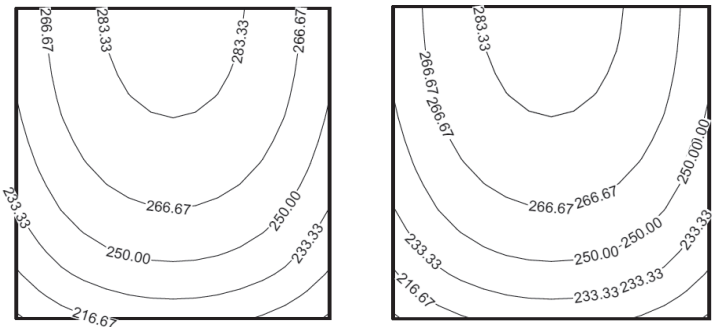

Figure 9: $D(F)_5$ (Pa) on Faces 1 and 2 for the case in 4.2.

In order to detect the influence of the grid size in the marching stability, the size of the obstacle is scaled to adjust to the ratio of $l_{\max}/\lambda$. Figure 12 shows the convergence histories for different ratios of $l_{\max}/\lambda$; meanwhile, the number of time steps is kept at 20. It is noted that the ratio of $l_{\max}/\lambda$ should be less than 0.027 in order to attain robust convergence.

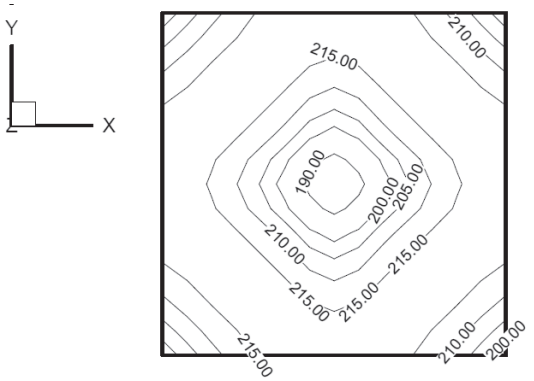

Figure 10: $D(F)_5$ (Pa) on Face 5 for the case in 4.2.

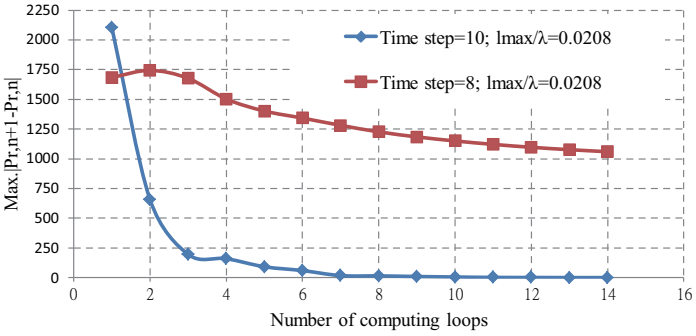

Figure 11: Convergence histories for the case in 4.3.

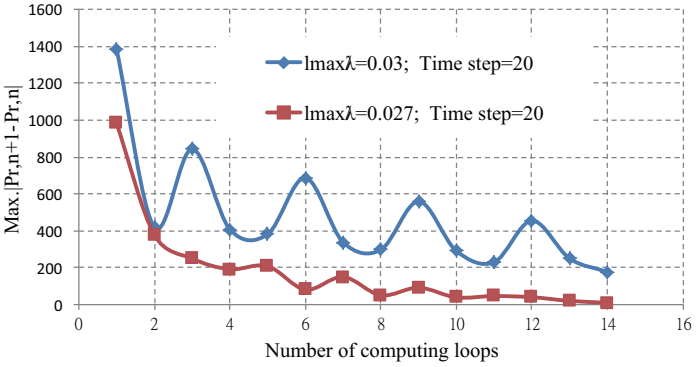

Figure 12: Convergence histories for the case in 4.3.

5 Conclusions

A step approach method derived in the time domain was developed for the time-harmonic radiating problem of an arbitrarily complex obstacle pulsating with multiple frequencies.

During the marching process, the boundary integral equation is expressed in forms relative to the retarded time, which makes the iteration process easier, and the radiated pressure on each element is updated by the source term (i.e. boundary condition) and the dipole term. The source term is known and associated with the vibration of the obstacle. The time interpolations in the dipole term are replaced by the Fourier series to reduce the numerical error. The initial radiated pressure on each element is set as zero.

The radiated pressure from a sphere pulsating with a monopole frequency in an infinite acoustic domain is solved, and when compared with the analytical solution is shown to be in good agreement. Then, a complex-shaped radiator composed of a cube and a pyramid in half-space is treated as the computing sample. The pulsating frequency imposed is multi-frequency. It is shown that a robust convergence can be obtained by means of the present method. With the present method, more than 10 time steps over the longest period are suggested, and the ratio of the maximum side length of the elements to the minima wave length, $l_{\max}/\lambda$, is required to be less than 0.027.

References

Araújo, F. C.; Mansur, W. J.; Carrer, J. A. M. (2000): Time-domain three-dimension analysis. *Boundary Element Acoustics*, edited by T. W. Wu (Southampton, UK, Boston, WIT Press, 2000). Chapter 8: pp. 59–216.

Bi, C. X.; Lin, G.; Zhang, X. Z. (2013): Cubic spline interpolation-based time-domain equivalent source method for modeling transient acoustic radiation. *Journal of Sound and Vibration*, vol. 332, no. 22, pp. 5939–5952.

Burton, A. J.; Miller, G. F. (1971): The application of integral equation methods to the numerical solution of some exterior boundary-value problems. *Proc. Roy. Soc. Lond. A.*, vol. 323, pp. 201–210.

Jin, C. (1993): A direct boundary integral equation method for the acoustic scattering problem. *Engineering Analysis with Boundary Elements*, vol. 12, pp. 39–46.

Dohner, J. L.; Shoureshi, R.; Bernhard, R. J. (1987): Transient analysis of three dimensional wave propagation using the boundary element method. *Int. J. Num. Methods in Eng.*, vol. 24, pp. 621–634.

Groenbroom, P. H. L. (1983): Wave propagation phenomena. *Progress in Boundary Elements Methods*, edited by C. A. Brebbia. vol. 2, no. Chapter 2, pp. 22–55.

Jang, H. W.; Ih, J. G. (2012): Stabilization of time domain acoustic boundary element method for the interior problem with impedance boundary conditions. *J. Acoust. Soc. Am*, vol. 131, pp. 2742–2752.

Kress, R.; Mohsen, A. (1986): On the simulation source technique for exterior problems in acoustics. *Math. Meth. In the Appl. Sci.*, pp. 585–597.

Kropp, W.; Svensson, P. U. (1995): Application of the time domain formulation of the method of equivalent sources to radiation and scattering problems. *Acta Acoustica*, vol. 81, pp. 528–543.

Li, W. L.; Wu, T. W.; Seybert, A. F. (1994): A half-space boundary element method for acoustic problems with a reflecting plane of arbitrary impedance. *J. Sound Vib.*, vol. 171, pp. 173–183.

Mansur, W. J.; Brebbia, C. A. (1982): Formulation of the boundary element method for transient problems governed by scalar wave equation. *Appl. Math. Modelling*, vol. 6, pp. 307–311.

Mikael, A. L.; Masami, N. (2013): Application of the time-domain boundary element method to analysis of flow-acoustic interaction in a hole-tone feedback system with a tailpipe. *Cmes-Computer Modeling in Engineering & Sciences*, vol. 96, no. 4, pp. 227–241.

Ochmann, M. (1995): The source simulation technique for acoustic radiation problems. *Acustica*, vol. 81, pp. 512–527.

Qian, Z. Y.; Han, Z. D.; Ufimtsev, P.; Atluri, S. N. (2004): Non-hypersingular boundary integral equations for acoustic problems, implemented by the collocation-based boundary element method. *Cmes-Computer Modeling in Engineering & Sciences*, vol. 6, no. 2, pp. 133–144.

Qian, Z. Y.; Han, Z. D.; Atluri, S. N. (2013): A fast regularized boundary integral method for practical acoustic problems. *Cmes-Computer Modeling in Engineering & Sciences*, vol. 91, no. 6, pp. 463–484.

Seybert, A. F.; Soenarko, B.; Rizzo, F. J.; Shippy, D. J. (1985): An advanced computational method for radiation and scattering of acoustic waves in three dimensions. *J. Acoust. Soc. Am.*, vol. 77, no. 2, pp. 362–368.

Seybert, A. F.; Soenarko, B. (1988): Radiation and scattering of acoustic waves from bodies of arbitrary shape in a three-dimensional half space. *ASME Trans.*, vol. 110, pp. 112–117.

Seybert, A. F.; Wu, T. W. (1988): Modified Helmholtz integral equation for bodies sitting on an infinite plane. *J. Acoust. Soc. Am.*, vol. 85, no. 1, pp. 19–23.

Schenck, H. A. (1968): Improved integral formulation for acoustic radiation problem. *J. Acoust. Soc. Am.*, vol. 44, no. 1, pp. 41–58.

Wu, T. W. (1994): On computational aspects of the boundary element for acoustic radiation and scattering in a perfect waveguide. *J. Acoust. Soc. Am.*, vol. 96, pp. 3733–3743.

Wu, T. W. (1995): A direct boundary element method for acoustic radiation and scattering from mixed regular and thin bodies. *J. Acoust. Soc. Am.*, vol. 97, pp. 84–91.

Zai, Y. Y. (2006): Treatment of sharp edges & corners in the acoustic boundary element method under neumann boundary condition. *Cmes-Computer Modeling in Engineering & Sciences*, vol. 13, no. 2, pp. 81–90.

Zhang, X. Z.; Bi, C. X.; Zhang, Y. B.; Xu, L. (2015): Sound source identification and sound radiation modeling in a moving medium using the time-domain equivalent source method. *J. Acoust. Soc. Am.*, vol. 137, no. 5, pp. 2678–2686.